This article has been accepted for publication in Journal of Lightwave Technology. This is the author's version which has not been fully edited and content may change prior to final publication. Citation information: DOI 10.1109/JLT.2025.3552855

S-Tapered Fluoride Optical Fiber for Refractive Index Sensing in the Mid-Infrared

Francesco Anelli, Sébastien Venck, Solenn Cozic, and Francesco Prudenzano, *Member, IEEE*

***Abstract*—This paper illustrates the first S-tapered optical fiber obtained by employing fluoride glass, via off-axis pulling and filament heating. The S-tapered optical fiber has been designed via three-dimensional beam propagation method and its performance with respect to the surrounding refractive index has been numerically predicted. The fabrication has been conducted using a commercial glass processor, operating at low power due to the glass thermal properties. The S-tapered optical fiber transmission spectrum has been measured in the mid-infrared when immersed in different surrounding liquids, i.e., methanol, ethanol, and propanol. A red shift of the dip in the transmission spectrum was observed for increasing values of the refractive index. Compared to the conventional wavelengths, expanding the functionality of optical fiber sensors to the mid-infrared spectrum has the potential to improve sensitivity.**

***Index Terms*—Optical fiber sensor, Optical fiber device, Fluoride glass, Mid-infrared, Refractive index**

I. Introduction

OPTICAL fiber sensors have gained significant attention due to their numerous advantages, such as immunity to electromagnetic interference, high sensitivity, small size, and ability to operate in harsh environments [1]. Some of the most common types of optical fiber sensors include Fiber Bragg Gratings (FBGs), Long Period Gratings (LPGs), and interferometric sensors [1]. FBGs are well-suited for quasi-distributed sensing applications due to their small size and punctual measurement. However, when used for refractive index (RI) measurements, FBGs often require additional treatments, which can significantly compromise their mechanical properties and long-term stability [2]. In contrast, LPG-based RI sensors are known for their robustness and high sensitivity, particularly when the surrounding RI is similar to that of the fiber cladding [2]. Nonetheless, both FBGs and LPGs typically necessitate precise and costly fabrication methods, such as phase mask techniques and high-cost laser sources [2]. Mach-Zehnder and Michelson interferometers for RI detection have been developed via non-adiabatic tapered optical fibers, obtained with a cheaper process based on heat-and-pull method via flame, CO_2 laser, or electric heaters [2], [3], [4], [5]. The non-adiabatic taper is employed to achieve the optical power exchange among the fundamental core mode and the cladding modes. The external physical quantity can be detected through the shift of the transmission spectrum [6]. Optical fiber sensors based on tapering offer several advantages, such as a straightforward design and cost efficiency [7], [8]. However, they tend to have relatively low RI sensitivities, and the length of the waist region is typically in the range of tens of millimeters, making them less suitable for compact integrated applications and quite fragile [2]. S-tapered optical fiber can be viewed as an improved miniaturized version of the fiber Mach-Zehnder interferometer based on non-adiabatic taper [2]. This structure was firstly developed in 2011 for RI and strain detection [9]. In 2013, a novel RI sensor based on S-tapered photonic crystal fibers was proposed as well as a S-taper in combination with a hybrid LPG to simultaneously measure both RI and temperature [10], [11]. Successively, different geometries have been investigated, e.g. double S-tapered fiber, optical fiber cascading [12], [13], S-tapered fiber coated with SiO_2 nanoparticles [8], and coated with graphene oxide [14], [15]. The S-tapered optical fiber has attracted considerable research interests in the measurement of different physical and biochemical parameters [16], including magnetic field [17], RI [10], temperature [11], [18], humidity [8], antigen–antibody interaction [19] etc. Most of the proposed sensors have been constructed using silica optical fibers due to their excellent thermo-mechanical properties and high transparency across ultra-violet to near-infrared wavelengths [20], [21]. However, silica glass has significant limitations, particularly its high attenuation at long wavelengths, which makes it unsuitable for transmitting light in the Mid-Infrared (Mid-IR) range with low

This work was partially supported by MIUR PRIN 2022, NRPP – DD n. 1181 del 27-07-2023 - InnoVative tEchnoloGies for non-invasivE assessmenT of plAnt healTh conditIon to support precisiOn farmiNg “VEGETATION” (P2022ZF9P2 , CUP: I53D23005710 001); H2020-ICT-37-2020 “Photonic Accurate and Portable Sensor Systems Exploiting Photo-Acoustic and Photo-Thermal Based Spectroscopy for Real-Time Outdoor Air Pollution Monitoring – PASSEPARTOUT” n. 101016956; the European Union under the Italian National Recovery and Resilience Plan (NRRP) of NextGenerationEU, with reference to the partnership on “Telecommunications of the Future” (PE00000001 - program “RESTART”, CUP: D93C22000910001) - STRUCTURAL PROJECT Antennas & Devices foR mixing, dEtection And Manipulation of mmWaves; ASI 687/2022 - MUR 341 15/03/22 “SPACE IT UP” (CUP: D53C24000570006); ASI 2024-68-I.0 “Origami Reconfigurable Beam-steering Antennas with METAsurfaces for Communication on Small Satellites - ORBIT-META” (CUP: F93C24000550001); HORIZON-TMA-MSCA-SE HORIZON TMA MSCA Staff Exchanges (101182995) “Cr4+:YAG/Polymer nanocomposite as alternative materials for Q-switched lasers: properties, modeling, and applications - ALTER-Q”.

This work did not involve human subjects or animals in its research.

Francesco Anelli, and Francesco Prudenzano are with the Department of Electrical and Information Engineering, Politecnico di Bari, 70125 Bari, Italy (e-mail: francesco.anelli@ poliba.it; francesco.prudenzano@poliba.it).

Sébastien Venck, and Solenn Cozic are with Le Verre Fluoré, 35170, Bruz, France (e-mail: sebastien.venck@leverrefluore.com; solenn.cozic@leverrefluore.com).

This article has been accepted for publication in Journal of Lightwave Technology. This is the author's version which has not been fully edited and content may change prior to final publication. Citation information: DOI 10.1109/JLT.2025.3552855

losses [22]. It is worth noting that Mid-IR region is very promising because it can allow higher sensitivity than conventional wavelengths, as detailed in Section II, and includes the most intense molecular absorption features [23], [24]. Glass materials such as fluoride and chalcogenide glasses can be considered for guiding light in the Mid-IR [25]. Fluoride glass exhibits a steep temperature viscosity profile near the glass transition temperature T_g, high thermal expansion coefficient, and tendency to devitrify. Nevertheless, at the moment, it is the glass offering the lowest attenuation from $\lambda = 2\ \mu m$ up to about $\lambda = 5\ \mu m$, good power handling capability, and low-phonon energy [26]. Therefore, despite the abovementioned challenges, developing optical fiber components on fluoride glass is very attractive [27].

In this paper, we present, for the first time to the best of our knowledge, the design, fabrication, and characterization of an S-tapered optical fiber based on zirconium fluoride glass (namely ZBLAN from its typical composition, i.e., 53% ZrF_4 - 20% BaF_2 - 4% LaF_3 - 3% AlF_3 - 20% NaF). In the design, a commercial three-dimensional beam propagation method is employed to explore the spectral properties and the sensitivity to surrounding RI of the S-tapered optical fiber. The fabrication is based on off-axis pulling under heating. The S-tapered optical fiber characterization shows a red-shift of the dip in the transmission spectrum, by increasing the surrounding RI. The proposed device can pave the way for other Mid-IR optical fiber sensors, particularly desirable for environmental monitoring and biomedical application to sense a wide variety of molecular species.

II. Operating Principle

As in the case of the non-adiabatic tapered sensor, the main concept behind the S-tapered optical fiber structure is to combine both interference arms, i.e., reference and sensing arm, within a single fiber [28].

Figure 1 illustrates a schematic diagram of the S-tapered optical fiber, consisting of the two input/output linear sections connected via two abrupt bends and a straight section among them [29]. Due to the presence of the first bend of the S-tapered region, high-order cladding modes are excited [8], [9], [30], [31]. The fundamental core mode and the high-order cladding modes travel through the intermediate straight section until they reach the second bend. At this point, the high-order cladding modes re-couple and interfere with the fundamental core mode [8], [9]. In the waist section, the cladding mode field extends outside the fiber and interacts with the surrounding medium, i.e. the environment, operating as the sensing arm, while the core mode remains confined within the fiber core. Since it is only slightly perturbed, it can serve as reference arm [28], [29]. This interaction can be described by the two-beam optical interference equation [32], [33]:

$$I_{out} = I_{co} + \sum_i I_{cl,i} + \sum_i 2 \times \sqrt{I_{co} \times I_{cl,i}} \times \cos(\Delta\phi_i) \qquad (1)$$

where I_{out}, I_{co}, and $I_{cl,i}$ are the output, core and i-th cladding mode intensities respectively, $\Delta\phi_i = 2\pi \times \Delta n_{eff,i} \times L_{eff}/\lambda$ is the phase difference between the core and i-th cladding mode, $\Delta n_{eff,i}$ is the effective RI difference between the core and i-th cladding mode, L_{eff} is the effective length of the S-taper, λ is the wavelength [28], [34]. Variation in external condition, such as temperature, strain, or RI, can alter $\Delta n_{eff,i}$ and/or L_{eff}, thereby altering the spectral properties of the S-tapered optical fiber and causing a shift of the resonance dip [28], [34]. The surrounding RI sensitivity of Mach-Zehnder interferometers based on optical fibers can be analytically derived, as demonstrated in [35], showing a direct proportionality between sensitivity and the wavelength λ. Similarly, also in the case of other optical fiber sensors, e.g. fiber Bragg grating, the sensitivity is proportional to the wavelength λ [36].

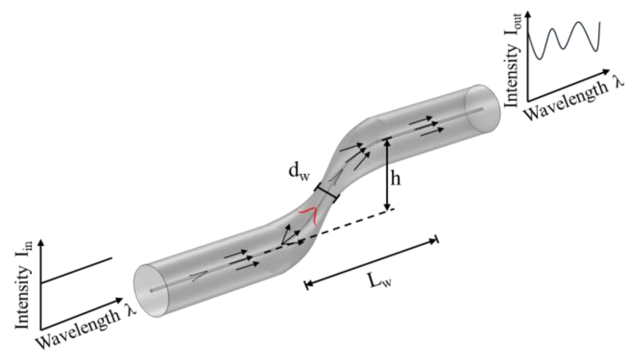

Fig. 1. Sketch of the S-tapered optical fiber: the power guided in the fundamental mode is partially coupled into the higher-order modes due to the S-taper. These modes then recombine, resulting in their interference and providing the characteristic of the Mach-Zehnder interferometer at the end of the optical fiber.

III. Design of the S-tapered zirconium fluoride optical fiber

A zirconium fluoride optical fiber, i.e. ZFG SM [1.95] 6.5/125, manufactured by Le Verre Fluoré in France, is employed. The core diameter is $d_{co} = 6.5\ \mu m$, the cladding diameter is $d_{cl} = 125\ \mu m$ and the numerical aperture is $NA = 0.23$. The cut-off wavelength for single-mode operation is $\lambda = 1.95\ \mu m$. To investigate the light propagation characteristics of the proposed S-tapered optical fiber, three-dimensional numerical simulation based on beam propagation method is performed via RSoft Design Group BeamPROP [30]. An exponential taper profile is employed to model the S-taper. Realistic RI dispersion as a function of the wavelength has been considered in the numerical design [37]. Three parameters can enable the optimization of the S-tapered optical fiber, i.e., waist diameter d_w, axial offset h, and tapered region length L_w, see Fig. 1 [34]. Several simulations were performed by varying these three parameters to increase sensor performance. In the simulation, the mesh size is $0.15\ \mu m \times 0.15\ \mu m$ in the transverse plane and $2.5\ \mu m$ in the longitudinal direction. The wavelength λ is swept in the range from $\lambda = 3000\ nm$ to $\lambda = 4000\ nm$ with a step $\Delta\lambda = 25\ nm$. The optimized taper dimensions are waist diameter $d_w = 65\ \mu m$, tapered region length $L_w = 1.4\ mm$, and axial offset $h = 130\ \mu m$, feasible with the glass processor.

This article has been accepted for publication in Journal of Lightwave Technology. This is the author's version which has not been fully edited and content may change prior to final publication. Citation information: DOI 10.1109/JLT.2025.3552855

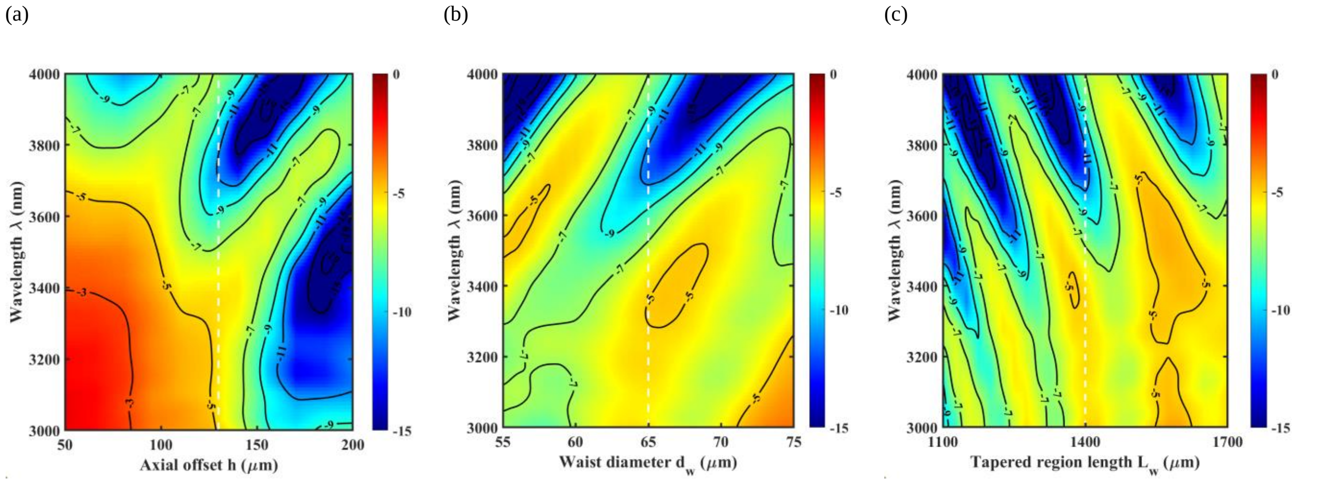

Fig. 2. Simulated transmission $T\ (dB)$ of the ZBLAN S-tapered optical fiber, as a function of the wavelength λ and of (a) the axial offsets h for waist diameter $d_w = 65\ \mu m$ and tapered region length $L_w = 1.4\ mm$, (b) the waist diameters d_w for axial offsets $h = 130\ \mu m$ and tapered region length $L_w = 1.4\ mm$, (c) the tapered region lengths L_w for axial offsets $h = 130\ \mu m$ and waist diameter $d_w = 65\ \mu m$. The optimized values are highlighted with a white dashed line.

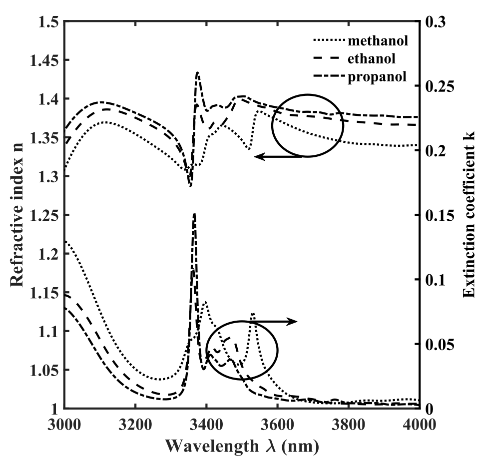

Fig. 3. Refractive index n and extinction coefficient k of methanol (dotted line), ethanol (dashed line), and propanol (dash-dotted line) as functions of the wavelength λ.

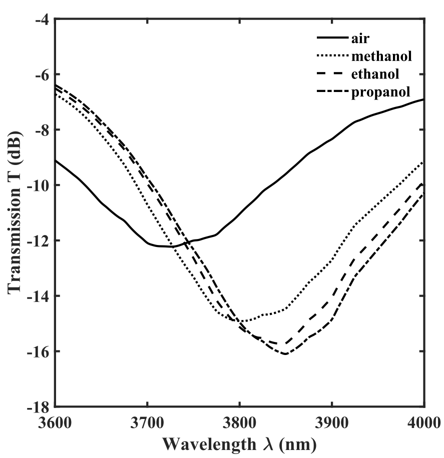

Fig. 4. Simulated transmission $T\ (dB)$, as a function of the wavelength λ for different surrounding materials, of the ZBLAN S-tapered optical fiber with waist diameter $d_w = 65\ \mu m$, waist length $L_w = 1.4\ mm$ and axial offset $h = 130\ \mu m$.

Figure 2 depicts the contour curves with colorimetric scale of the transmission T in dB, calculated as the ratio among the power guided by the LP_{01} mode at the output section and the input power varying one of the optimized parameters while keeping the other two constant. This figure refers to the S-tapered optical fiber surrounded by air. In particular, Fig. 2 (a) illustrates the axial offset h variation in the range from $h = 50\ \mu m$ to $h = 200\ \mu m$ with a step $\Delta h = 15\ \mu m$, Fig. 2 (b) the waist diameter d_w variation in the range from $d_W = 55\ \mu m$ to $d_w = 75\ \mu m$ with a step $\Delta d_w = 1\ \mu m$, while Fig. 2 (c) the tapered region length L_w variation in the range from $L_w = 1100\ \mu m$ to $L_w = 1700\ \mu m$ with a step $\Delta L_w = 25\ \mu m$. For small axial offset h, the electromagnetic field is not efficiently coupled with the higher order modes and, thus, the output spectrum does not present any spectral interference pattern. On the contrary, when the axial offset h is very large ($h > 200\ \mu m$), part of the optical power energy is dissipated as bending loss, and the remaining optical power of the fundamental mode and higher-order modes participating in the interference process decreases [29].

As is widely known, the S-tapered optical fiber is sensitive to the real part of the surrounding RI, leading overall to a shift in the transmission spectrum and to a change of transmission due to a variation of optical beam confinement. For this analysis, three measurand substances, i.e. surrounding environment, are considered. Figure 3 reports the RI n and the extinction coefficient k as functions of the wavelength λ of the measurand substances then considered in the experiment: methanol (dotted line), ethanol (dashed line), and propanol (dash-dotted line) [38]. The axial offset $h = 130\ \mu m$ is chosen since it results in a reduced waveguide transmission level at approximately $\lambda = 3700\ nm$, as illustrated in Fig. 2, where the extinction coefficients k of the measurand substances are small and the RI changes among them are large, see Fig. 3. The low transmission can be ascribed to the strong evanescent field of the cladding modes and their destructive interference with the core mode.

Figure 4 reports the simulated transmission $P_{out}(dB)$ as a function of the wavelength λ of the zirconium fluoride S-

This article has been accepted for publication in Journal of Lightwave Technology. This is the author's version which has not been fully edited and
content may change prior to final publication. Citation information: DOI 10.1109/JLT.2025.3552855

tapered optical fiber, referring to the case with waist diameter $d_w = 65\ \mu m$, waist length $L_w = 1.4\ mm$, and axial offset $h = 130\ \mu m$. For the sake of clarity, the solid line in Fig. 4 corresponds to the white dashed lines in Fig. 2, pertaining to the case of air as surrounding medium. These simulations have been performed with a wavelength sampling step $\Delta\lambda = 5\ nm$ in the wavelength range from $\lambda = 3600\ nm$ to $\lambda = 4000\ nm$ and with a sampling step $\Delta\lambda = 1\ nm$ in the wavelength range of about $20\ nm$ around the resonance dip for each surrounding material, i.e. air, methanol, ethanol, and propanol. A redshift of the dip is obtained by increasing the RI of the surrounding medium. In particular, the simulated transmission dip wavelength is $\lambda_{air} = 3726\ nm$, $\lambda_{meth} = 3802\ nm$, $\lambda_{eth} = 3844\ nm$, $\lambda_{pro} = 3850\ nm$ for air, methanol, ethanol, and propanol, respectively. Thus, the maximum wavelength shift occurs when considering propanol, i.e., for the largest RI, and it is approximately $\Delta\lambda = 124\ nm$. A monotonically decreasing trend of the transmitted power by increasing the surrounding RI is observed. This is justified by a lower field confinement, since all the measurand substances exhibit low extinction coefficient k in the considered wavelength range.

IV. Fabrication of the S-tapered zirconium fluoride optical fiber

The device is fabricated by applying off-axis pull while tapering the single-mode zirconium fluoride optical fiber, i.e. ZFG SM [1.95] 6.5/125 from Le Verre Fluoré (Bruz, France), with the automated glass processing system Vytran GPX-2400 [2], [39]. Since fluoride optical fibers are not compatible with common stripping tools, a stripping gel is employed to remove the coating. Then, the optical fiber is cleaved with an automatic cleaver, based on tension-and-scribe process, with a tension $L = 95\ g$, and carefully cleaned with propanol. After, the optical fiber is mounted on the fiber holders and axial offset is provided, as schematically illustrated in Fig. 5.

The process continues with a pre-tension, obtained via the movement of one fiber holder. The main process consists of two main parts: heating and pulling. The commercial graphite filament is switched on and set to operate near the glass transition temperature T_g of the zirconium fluoride glass.

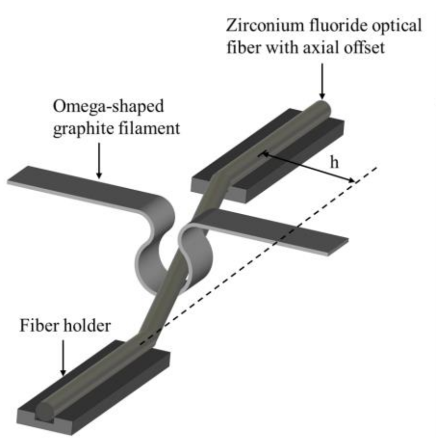

Fig. 5. Sketch of the fabrication process: an axially offset zirconium fluoride fiber segment, clamped in fiber holders, is stretched while being heated by the graphite filament at a temperature close to the glass transition temperature T_g.

At the same time, the feeding speed is lower than the pulling speed as to provide the necessary tensile strain to reduce the optical fiber diameter. The glass transition temperature T_g of the zirconium fluoride optical fiber has been identified by measuring its viscosity as a function of temperature T with a parallel plates viscosimeter Theta model Rheotronic III. Glass cylinders with diameter $d \simeq 7\ mm$ and height $h_{cyl} \simeq 7\ mm$ were fabricated and employed in the measurement with an applied load of $50\ g$. The measurement was performed from room temperature to $T_g + 100\ °C$ with a heating rate of *10 °C/min* up to $T_g - 50\ °C$ and $3\ °C/min$ up to $T_g + 100\ °C$. The temperature and the sample height were recorded every 50 seconds. The viscosity was then calculated [40]. In particular, T_g marks the point at which the material begins to soften due to a higher molecular mobility and is identified as the point where viscosity sharply decreases. Figure 6 shows a very steep reduction in viscosity beyond T_g which confirms the well-known zirconium fluoride glass fragility, highlighting that even minor temperature fluctuations around T_g can dramatically alter viscosity and potentially compromise the drawing quality [41], [42]. To address this sensitivity, precise temperature control is required for achieving the desired dimensions and low losses. The temperature at which the glass is drawn is crucial for the S-taper fabrication but, at the same time, challenging to be precisely determined, as it depends on several parameters which include filament power, heating time, and fiber holding block velocity. Monitoring tension during the fabrication and analyzing micrographs helps optimize fabrication parameters, preventing defects like crystallization, or taper failure.

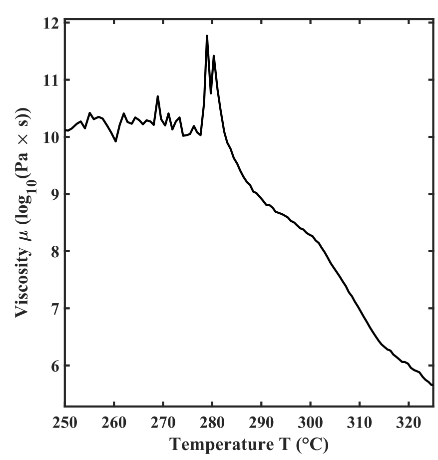

Fig. 6. Viscosity μ of zirconium fluoride glass as a function of temperature T.

Fig. 7. Longitudinal view of the fabricated zirconium fluoride S-tapered optical fiber taken via Vytran GPX-2400 CCD camera.

This article has been accepted for publication in Journal of Lightwave Technology. This is the author's version which has not been fully edited and content may change prior to final publication. Citation information: DOI 10.1109/JLT.2025.3552855

Figure 7 reports four micrographs of the S-tapered zirconium fluoride optical fiber longitudinal view taken with the CCD camera of Vytran GPX-2400. In particular, each micrograph spans an area of $800\ \mu m$. A good agreement with the designed geometry is obtained. Moreover, when considering soft glasses and especially with fluoride glasses, it is important to pay attention to the eventual presence of a grainy texture that indicates that the glass was over softened, and crystals were formed [43]. By inspecting these micrographs, it is possible to conclude that a successful fabrication is obtained. Furthermore, the high-quality transitions in Fig. 7 suggest heating near the glass transition temperature T_g.

V. Characterization of the S-tapered zirconium fluoride optical fiber and performance comparison

A. Characterization of the S-tapered optical fiber

The experimental setup for the characterization of the proposed S-tapered zirconium fluoride optical fiber consists of broadband halogen source Osram 64633 HLX, InSb InfraRed Associates Inc. detector, and Horiba iHR 550 monochromator. One end of the S-tapered optical fiber is aligned with the single-mode zirconium fluoride injection fiber delivering the broadband halogen source power, the other end with the detector, in order to monitor the output power. To ensure that before the S-taper only the fundamental mode is guided, a long injection fiber was used, coated with a high-refractive index resin. To radiate all the power guided by the cladding modes after the S-taper, the same polymer coating, operating as a cladding mode stripper, is employed, this ensuring the measurement only of the fundamental mode.

The measured transmission spectrum is reported in Fig. 8. A maximum attenuation at $\lambda = 3755\ nm$ is obtained for the sensor operating in air. Then, the sensor is immersed in different liquids. After recording the transmission spectrum for each liquid, the S-tapered zirconium fluoride optical fiber was cleaned with propanol and dried with compressed air to restore its original spectrum in air [2]. As it is indicated by simulations, red shift is obtained when the sensor is immersed in the measurand substances. The shift increases progressively from methanol, which has the lowest RI, to propanol, which has the highest, in agreement with the simulation results shown in Fig. 2. Also in the measurement, higher attenuation is obtained for positive changes of the surrounding RI. The measured transmission spectra for air and the three measurand substances show slight deviations from the simulation results. In particular, measured and simulated spectra exhibit almost the same maximum wavelength shift $\Delta\lambda$. The measured attenuation exceeds theoretical predictions. This discrepancy can be attributed to several factors, including that the measured transmission accounts for coupling loss and propagation losses not considered in the theoretical model. Additionally, surface imperfections or roughness may contribute to increased scattering losses, leading to higher attenuation.

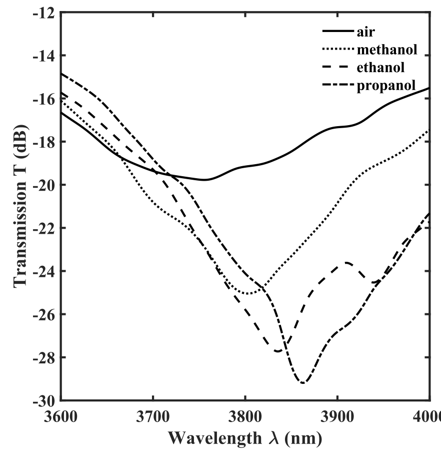

Fig. 8. Measured transmission $T(dB)$ as a function of the wavelength λ for different surroundings, i.e., air (solid line), methanol (dotted line), ethanol (dashed line), and propanol (dash-dotted line).

B. Performance comparison and discussion

Table I reports a comparison with other literature RI optical fiber sensor based on a similar configuration. These sensors are based on silica optical fiber and operate in the near infrared. It can be noticed that the wavelength shift $\Delta\lambda$, and thus, the sensitivity of the proposed sensor is higher than most sensors, even when based on more complex configurations or requiring a more expensive or time-consuming fabrication process.

TABLE I
COMPARISON WITH LITERATURE RI OPTICAL FIBER SENSORS BASED ON SIMILAR STRUCTURES

Ref.	Structure	Wavelength Shift Δλ (RI interval)
[2]	Single S-tapered optical fiber	$\simeq 50\ nm$ (1.33 ÷ 1.42)
[9]	Single S-tapered optical fiber	$\simeq 55\ nm$ (1.33 ÷ 1.43)
[10]	Single S-tapered photonic crystal optical fiber	$\simeq 12\ nm$ (1 ÷ 1.44)
[11]	Long period grating cascaded to S-tapered optical fiber	$\simeq 13\ nm$ (1.333 ÷ 1.373)
[29]	Single S-tapered optical fiber	$\simeq 6\ nm$ (1.335 ÷ 1.345)
[44]	Single S-tapered optical fiber liquid-sealed in a capillary	$\simeq 60\ nm$ (1.34 ÷ 1.42)
[45]	Single S-tapered optical fiber with silver mirror	$\simeq 55\ nm$ (1.33 ÷ 1.43)
[46]	Cascade of two single-mode optical fiber tapers	$\simeq -0.8\ nm$ (1.3515 ÷ 1.36)
[47]	Micro-deformed tapered loop optical fiber with a ball-shaped optical fiber end	$\simeq 65\ nm$ (1.3 ÷ 1.34)
[48]	Non-adiabatic tapered optical fiber with $6 \div 8\ \mu m$ waist diameter into a fiber loop mirror configuration	$\simeq 16\ nm$ (1.338 ÷ 1.351)
[49]	Tapered long period grating	$\simeq 38\ nm$ (1.3 ÷ 1.37)
[50]	Step-index optical fiber spliced on both ends of a tapered photonic crystal optical fiber	$\simeq 9.5\ nm$ (1.335 ÷ 1.3825)
This paper	Single S-tapered ZBLAN optical fiber operating in the Mid-IR spectral range	$\simeq 47\ nm$ (1 ÷ 1.3430) $\simeq 33\ nm$ (1.3430 ÷ 1.3697) $\simeq 107\ nm$ (1 ÷ 1.3781)

It is worth noting that with these sensors, the sensitivity is not linear and becomes higher when the surrounding RI approaches the cladding RI. Future work could explore various zirconium fluoride fiber geometries to achieve more pronounced dips, enhancing measurement accuracy also to parity of wavelength shift. Additionally, by utilizing detectors such as optical spectrum analyzers/spectrometers with very low minimum detectable power per nanometer, the optical fiber sensor can be designed and optimized to operate within the specific wavelength range where analytes exhibit absorption. This approach would fully exploit the characteristic molecular absorption peaks in the Mid-IR range. Such sensors could be fabricated using techniques similar to those outlined in this paper, enabling the investigation of low concentrations by leveraging the extinction coefficient k of the target substances. To conclude, this paper presents an S-tapered zirconium fluoride optical fiber for sensing applications, investigating the shift in the output spectrum as a function of the surrounding RI. The key objective of the paper is to investigate the feasibility of developing optical fiber sensors based on fluoride glasses. The related advantages include: (i) the ability to extend sensing functionality to longer wavelengths, enhancing sensitivity as discussed in Section II; (ii) the improvement of temperature sensitivity in cryogenic environments [51]; (iii) the application in molecular absorption-based spectroscopy; and (iv) the potential integration of silica and fluoride-based sensors within multiparameter sensing networks for enhanced compensation and versatility.

VI. Conclusions

The paper presented the first zirconium fluoride S-tapered optical fiber for RI sensing in the Mid-IR spectral range. The optical fiber sensor has been designed via three-dimensional beam propagation method, estimating also the shift of the transmission spectrum dip versus different surrounding liquids, i.e., methanol, ethanol, and propanol. The S-taper has been fabricated via glass processing system based on pulling and graphite filament heating, obtaining good transition quality and overcoming the glass challenges related to mechanical fragility, steep viscosity/temperature profile, large thermal expansion coefficient, and crystallization issues. The characterization proves the possibility to perform high-sensitivity RI monitoring in the Mid-IR, surpassing the performance of similar sensors based on the conventional silica glass operating in the near infrared spectral range. A wavelength shift $\Delta\lambda = 107\,nm$ has been measured when considering propanol instead of air as surrounding environment, in good agreement with the numerical results. This work can open new avenues for advanced sensor technologies and practical applications in real-world scenarios.

Acknowledgment

The authors would like to thank Dr. Ronan Lebullenger (Univ. Rennes, France) for his contribution to viscosity measurement.

References

[1] M. Elsherif *et al.*, "Optical Fiber Sensors: Working Principle, Applications, and Limitations," *Adv. Photonics Res.*, vol. 3, no. 11, p. 2100371, Nov. 2022, doi: 10.1002/adpr.202100371.

[2] R. Yang *et al.*, "S-Tapered Fiber Sensors for Highly Sensitive Measurement of Refractive Index and Axial Strain," *J. Light. Technol.*, vol. 30, no. 19, pp. 3126–3132, Oct. 2012, doi: 10.1109/JLT.2012.2210997.

[3] M. Lakomski, B. Guzowski, and A. Wozniak, "Fabrication of ultra-long tapered optical fibers," *Microelectron. Eng.*, vol. 221, p. 111193, Jan. 2020, doi: 10.1016/j.mee.2019.111193.

[4] N. A. Razak, B. A. Hamida, N. Irawati, and M. H. Habaebi, "Fabricate Optical Microfiber by Using Flame Brushing Technique and Coated with Polymer Polyaniline for Sensing Application," *IOP Conf. Ser. Mater. Sci. Eng.*, vol. 210, p. 012041, Jun. 2017, doi: 10.1088/1757-899X/210/1/012041.

[5] X. Yi *et al.*, "CO_2 Laser Tapering of Intrinsic Fabry–Perot Interferometers for Sensing," *IEEE Sens. J.*, vol. 23, no. 6, pp. 5824–5830, Mar. 2023, doi: 10.1109/JSEN.2023.3241046.

[6] X. Huang *et al.*, "An in-line Mach-Zehnder Interferometer Using Thin-core Fiber for Ammonia Gas Sensing With High Sensitivity," *Sci. Rep.*, vol. 7, no. 1, p. 44994, Apr. 2017, doi: 10.1038/srep44994.

[7] W. Zhang *et al.*, "Advances in Tapered Optical Fiber Sensor Structures: From Conventional to Novel and Emerging," *Biosensors*, vol. 13, no. 6, p. 644, Jun. 2023, doi: 10.3390/bios13060644.

[8] H. Liu *et al.*, "Relative Humidity Sensor Based on S-Taper Fiber Coated With SiO_2 Nanoparticles," *IEEE Sens. J.*, vol. 15, no. 6, pp. 3424–3428, Jun. 2015, doi: 10.1109/JSEN.2015.2389519.

[9] R. Yang *et al.*, "Single S-tapered fiber Mach–Zehnder interferometers," *Opt. Lett.*, vol. 36, no. 23, p. 4482, Dec. 2011, doi: 10.1364/OL.36.004482.

[10] F. Shi, J. Wang, Y. Zhang, Y. Xia, and L. Zhao, "Refractive Index Sensor Based on S-Tapered Photonic Crystal Fiber," *IEEE Photonics Technol. Lett.*, vol. 25, no. 4, pp. 344–347, Feb. 2013, doi: 10.1109/LPT.2013.2238623.

[11] J. Li *et al.*, "Long-Period Fiber Grating Cascaded to an S Fiber Taper for Simultaneous Measurement of Temperature and Refractive Index," *IEEE Photonics Technol. Lett.*, vol. 25, no. 9, pp. 888–891, May 2013, doi: 10.1109/LPT.2013.2255035.

[12] S.-C. Yan, Y. Zhao, M.-Q. Chen, and Q. Liu, "Optical fiber strain sensor with double S-tapers," *Instrum. Sci. Technol.*, vol. 49, no. 3, pp. 313–326, May 2021, doi: 10.1080/10739149.2020.1840387.

[13] W.-M. Zhao and Q. Wang, "A high sensitivity refractive index sensor based on three-level gradient structure S-tapered fiber mode-mode interferometer," *Measurement*, vol. 139, pp. 49–60, Jun. 2019, doi: 10.1016/j.measurement.2019.03.018.

[14] Y. Zhao *et al.*, "Relative humidity sensor of S fiber taper based on graphene oxide film," *Opt. Commun.*, vol. 450, pp. 147–154, Nov. 2019, doi: 10.1016/j.optcom.2019.05.072.

[15] Z. Lv, P. Niu, J. Jiang, S. Wang, Y. Liu, and T. Liu, "Reflective SFT-FBG Hybrid Micro-Probe for Simultaneous Measurement of Relative Humidity and Temperature," *IEEE Photonics J.*, vol. 14, no. 1, pp. 1–6, Feb. 2022, doi: 10.1109/JPHOT.2021.3136677.

[16] X. Hu, H. Zhang, W. Lin, T. Liu, and B. Liu, "Light-Controlled Asymmetric Dual-S-Taper Fiber Interferometer Integrated With Ethyl Orange Solution Under 473 nm Laser Illumination," *IEEE Sens. J.*, vol. 21, no. 21, pp. 24149–24156, Nov. 2021, doi: 10.1109/JSEN.2021.3113567.

[17] M. Deng, D. Liu, and D. Li, "Magnetic field sensor based on asymmetric optical fiber taper and magnetic fluid," *Sens. Actuators Phys.*, vol. 211, pp. 55–59, May 2014, doi: 10.1016/j.sna.2014.02.014.

[18] J. Ma, S. Wu, H. Cheng, X. Yang, S. Wang, and P. Lu, "Sensitivity-enhanced temperature sensor based on encapsulated S-taper fiber Modal interferometer," *Opt. Laser Technol.*, vol. 139, p. 106933, Jul. 2021, doi: 10.1016/j.optlastec.2021.106933.

[19] S. Duan *et al.*, "Hydrophobin HGFI–based fibre-optic biosensor for detection of antigen–antibody interaction," *Nanophotonics*, vol. 9, no. 1, pp. 177–186, Jan. 2020, doi: 10.1515/nanoph-2019-0370.

[20] C. Holmes, M. Godfrey, P. L. Mennea, S. Zahertar, and J. M. Dulieu-Barton, "Flexible photonics in low stiffness doped silica for use in fibre reinforced polymer composite materials," *Opt. Mater.*, vol. 134, p. 113133, Dec. 2022, doi: 10.1016/j.optmat.2022.113133.

[21] G. Wang, Z. Li, J. Wang, J. Shen, M. Zhang, and M. Huang, "Fabrication and sensing characterization of an S-tapered fiber probe,"

AIP Adv., vol. 10, no. 7, p. 075306, Jul. 2020, doi: 10.1063/5.0005456.

[22] M. Rezaei, G. T. Zeweldi, M. H. M. Shamim, and M. Rochette, "Single-mode optical fiber couplers made of fluoride glass," *Opt. Express*, vol. 31, no. 17, p. 27183, Aug. 2023, doi: 10.1364/OE.495464.

[23] E. Vicentini, A. Gambetta, F. Canella, N. Coluccelli, P. Laporta, and G. Galzerano, "High-resolution mid-infrared spectroscopy based on ultrafast Cr:ZnSe laser," *Opt. Express*, vol. 31, no. 13, p. 21482, Jun. 2023, doi: 10.1364/OE.491397.

[24] K. Kinjalk *et al.*, "Highly selective and sensitive detection of volatile organic compounds using long wavelength InAs-based quantum cascade lasers through quartz-enhanced photoacoustic spectroscopy," *Appl. Phys. Rev.*, vol. 11, no. 2, p. 021427, Jun. 2024, doi: 10.1063/5.0189501.

[25] V. S. Shiryaev, A. P. Velmuzhov, T. V. Kotereva, E. A. Tyurina, M. V. Sukhanov, and E. V. Karaksina, "Recent Achievements in Development of Chalcogenide Optical Fibers for Mid-IR Sensing," *Fibers*, vol. 11, no. 6, p. 54, Jun. 2023, doi: 10.3390/fib11060054.

[26] A. Séguin, R. I. Becerra-Deana, S. Virally, C. Boudoux, and N. Godbout, "Fabrication and characterization of indium fluoride multimode fused fiber couplers for the mid-infrared," *Opt. Express*, vol. 31, no. 20, p. 33670, Sep. 2023, doi: 10.1364/OE.501849.

[27] F. Anelli, A. Annunziato, A. M. Loconsole, S. Venck, S. Cozic, and F. Prudenzano, "Mode-Group Selective Photonic Lantern based on Indium Fluoride Optical Fibers for Mid-Infrared," *J. Light. Technol.*, pp. 1–8, 2024, doi: 10.1109/JLT.2024.3450115.

[28] L. Xiao *et al.*, "Development and stability analysis of an S-tapered optical fiber-based sensor structure," *Appl. Opt.*, vol. 62, no. 16, p. E37, Jun. 2023, doi: 10.1364/AO.483335.

[29] H. Liu *et al.*, "Temperature-Insensitive Label-Free Sensors for Human IgG Based on S-Tapered Optical Fiber Sensors," *IEEE Access*, vol. 9, pp. 116286–116293, 2021, doi: 10.1109/ACCESS.2021.3106343.

[30] X. Zhang *et al.*, "Label-Free Detection of DNA Hybridization Utilizing Dual S-Tapered Thin-Core Fiber Interferometer," *J. Light. Technol.*, vol. 37, no. 11, pp. 2762–2767, Jun. 2019, doi: 10.1109/JLT.2018.2864798.

[31] B. Wang *et al.*, "Mach–Zehnder Interferometer Based on S-Tapered All-Solid Photonic Bandgap Fiber," *IEEE Photonics Technol. Lett.*, vol. 27, no. 17, pp. 1849–1852, Sep. 2015, doi: 10.1109/LPT.2015.2443861.

[32] T. Zhou, Y. Zhang, B. Han, A. Zhang, and D. Fu, "Low cost non-adiabatic tapered fiber for high-sensitive temperature sensing," *Opt. Fiber Technol.*, vol. 45, pp. 53–57, Nov. 2018, doi: 10.1016/j.yofte.2018.06.004.

[33] R. Wang *et al.*, "Highly Sensitive Curvature Sensor Using an In-Fiber Mach–Zehnder Interferometer," *IEEE Sens. J.*, vol. 13, no. 5, pp. 1766–1770, May 2013, doi: 10.1109/JSEN.2013.2243834.

[34] J. Jiang *et al.*, "S-Taper Fiber Based Moisture Sensing in Power Transformer Oil," *IEEE Trans. Instrum. Meas.*, vol. 72, pp. 1–8, 2023, doi: 10.1109/TIM.2023.3246474.

[35] W. Liu *et al.*, "Refractive index and temperature sensor based on Mach-Zehnder interferometer with thin fibers," *Opt. Fiber Technol.*, vol. 54, p. 102101, Jan. 2020, doi: 10.1016/j.yofte.2019.102101.

[36] H. Alemohammad, "Opto-Mechanical Modeling of Fiber Bragg Grating Sensors," in *Opto-Mechanical Fiber Optic Sensors*, Elsevier, 2018, pp. 1–26. doi: 10.1016/B978-0-12-803131-5.00001-5.

[37] F. Anelli, A. Annunziato, A. M. Loconsole, P. L. Pays Du Teilleul, S. Cozic, and F. Prudenzano, "LPG in Fluoride Optical Fiber via Micro-Tapering Technique: Mid-IR Mode Coupling," *J. Light. Technol.*, pp. 1–8, 2024, doi: 10.1109/JLT.2024.3496501.

[38] T. L. Myers *et al.*, "Accurate Measurement of the Optical Constants *n* and *k* for a Series of 57 Inorganic and Organic Liquids for Optical Modeling and Detection," *Appl. Spectrosc.*, vol. 72, no. 4, pp. 535–550, Apr. 2018, doi: 10.1177/0003702817742848.

[39] K. Tian, M. Zhang, G. Farrell, R. Wang, E. Lewis, and P. Wang, "Highly sensitive strain sensor based on composite interference established within S-tapered multimode fiber structure," *Opt. Express*, vol. 26, no. 26, p. 33982, Dec. 2018, doi: 10.1364/OE.26.033982.

[40] A. K. Varshneya and J. C. Mauro, "The viscosity of glass," in *Fundamentals of Inorganic Glasses*, Elsevier, 2019, pp. 215–251. doi: 10.1016/B978-0-12-816225-5.00009-2.

[41] C. A. Angell, "Spectroscopy simulation and scattering, and the medium range order problem in glass," *J. Non-Cryst. Solids*, vol. 73, no. 1–3, pp. 1–17, Aug. 1985, doi: 10.1016/0022-3093(85)90334-5.

[42] V. N. Novikov, Y. Ding, and A. P. Sokolov, "Correlation of fragility of supercooled liquids with elastic properties of glasses," *Phys. Rev. E*, vol. 71, no. 6, p. 061501, Jun. 2005, doi: 10.1103/PhysRevE.71.061501.

[43] É. Ducharme, S. Virally, R. I. Becerra-Deana, C. Boudoux, and N. Godbout, "Viscosity of fluoride glass fibers for fused component fabrication," *Appl. Opt.*, vol. 61, no. 17, p. 5031, Jun. 2022, doi: 10.1364/AO.455528.

[44] R. Yang *et al.*, "A Highly Sensitive Temperature Sensor Based on a Liquid-Sealed S-Tapered Fiber," *IEEE Photonics Technol. Lett.*, vol. 25, no. 9, pp. 829–832, May 2013, doi: 10.1109/LPT.2013.2252336.

[45] C. Chen *et al.*, "Compact refractive index sensor based on an S-tapered fiber probe," *Opt. Mater. Express*, vol. 8, no. 4, p. 919, Apr. 2018, doi: 10.1364/OME.8.000919.

[46] Z. Tian *et al.*, "Refractive Index Sensing With Mach–Zehnder Interferometer Based on Concatenating Two Single-Mode Fiber Tapers," *IEEE Photonics Technol. Lett.*, vol. 20, no. 8, pp. 626–628, Apr. 2008, doi: 10.1109/LPT.2008.919507.

[47] L. F. Enriquez-Gomez *et al.*, "Micro-Deformed Looped Fiber Taper With High Sensitivity to Refractive Index," *IEEE Photonics Technol. Lett.*, vol. 32, no. 2, pp. 93–96, Jan. 2020, doi: 10.1109/LPT.2019.2958270.

[48] M. I. Zibaii, O. Frazao, H. Latifi, and P. A. S. Jorge, "Controlling the Sensitivity of Refractive Index Measurement Using a Tapered Fiber Loop Mirror," *IEEE Photonics Technol. Lett.*, vol. 23, no. 17, pp. 1219–1221, Sep. 2011, doi: 10.1109/LPT.2011.2158641.

[49] T. Allsop *et al.*, "Spectral characteristics of tapered LPG device as a sensing element for refractive index and temperature," *J. Light. Technol.*, vol. 24, no. 2, pp. 870–878, Feb. 2006, doi: 10.1109/JLT.2005.862426.

[50] R. Fan *et al.*, "Liquid Level and Refractive Index Double-Parameter Sensor Based on Tapered Photonic Crystal Fiber," *J. Light. Technol.*, vol. 38, no. 14, pp. 3717–3722, Jul. 2020, doi: 10.1109/JLT.2020.2975814.

[51] K. Grebnev, A. Sultanov, G. Oelsner, I. Chiamenti, and M. Chernysheva, "Thermal properties of fluoride fiber Bragg gratings at high to cryogenic temperatures," *Opt. Lett.*, vol. 49, no. 22, p. 6589, Nov. 2024, doi: 10.1364/OL.545902.

Francesco Anelli received the Ph.D. degree in electrical and information engineering from Politecnico di Bari, Bari, Italy, in 2024. He is currently a researcher at Politecnico di Bari. His research interests include fluoride fused optical fiber components for mid-infrared applications.

Sébastien Venck is currently with Le Verre Fluoré. His research interests include Mid-Infrared fiber-based supercontinuum laser source, ICL and QCL pigtailing with fluoride and chalcogenide optical fibers.

Solenn Cozic received the Ph.D. degree in material science from Rennes 1 University, Rennes, France, in 2016. She is currently a Research and Development Engineer with Le Verre Fluoré. Her research interests include development of novel fluoride glasses, optical fibers, and fluoride glass fiber components for mid infrared, and visible fiber lasers applications.

Francesco Prudenzano (Member, IEEE) received the Ph.D. degree in electronic engineering from the Politecnico di Bari, Bari, Italy, in November 1996. Since 2018, he has been a Full Professor of electromagnetic fields in the Department of Electrical and Information Engineering at the Politecnico di Bari. Since October 2024, he has served as the Head of the Department of Electrical and Information Engineering at the Politecnico di Bari. His research interests include the design and characterization of microwave devices, integrated optics, and optical fiber-based devices. He is the Head of Microwave and Optical Engineering Group, Politecnico di Bari. From 2017 to 2018, he served as the Chair of SIOF, the Italian Society of Optics and Photonics. He has coauthored more than 410 publications, 300 of which were published in journals and international conferences, lectures, and invited papers. He is involved in several national and international research projects and cooperations.